International Journal of Robotics and Control Systems
Vol. 6, No. 2, 2026, pp. 1060-1078
ISSN 2775-2658
http://pubs2.ascee.org/index.php/ijrcs

Optimal Frequency Regulation Control Based on Nonlinear Hybrid Controller for Iraqi Interconnected Power System

Mazin N. Ajaweed [a,1,*], Abbas H. Issa [b,2], Mazin T. Muhssin [c,3]

[a] Artificial Intelligence Engineering College, University of Technology, Baghdad, Iraq
[b] Electrical Engineering College, University of Technology, Baghdad, Iraq
[c] Power Engineering Department, Mustansiriya University, Baghdad, Iraq
[1] mazin.n.ajaweed@uotechnology.edu.iq; [2] abbas.h.issa@uotechnology.edu.iq; [3] mazintm@uomustansiriyah.edu.iq
* Corresponding Author

ARTICLE INFO

Article history
Received December 31, 2025
Revised January 31, 2026
Accepted April 08, 2026

Keywords
Three-Areas;
Interconnected Power System;
Hybrid Optimized Fractional Order Sliding Mode Controller (HOFOSMC);
Optimized Fractional Order Sliding Mode Controller (OFOSMC)

ABSTRACT

This study investigates critical challenges associated with Load Frequency Control (LFC) in interconnected power system using a realistic model of the Iraqi three-area interconnected power system. In this paper, these areas include the power system northern, central, and southern regions each comprising different power sources generation, including hydro, thermal, gas, and diesel units. The model is calibrated based on physical real data supplied by the ministry of electricity in Iraq. In addition, this study considers improving the performance of the nonlinear conventional fractional sliding mode controller by incorporating an additional switching function alongside with the traditional switching function to mitigate the steady-state error and oscillations accompanying the LFC system. Thus, the modified controller is hereafter called Hybrid Optimized Fractional Order Sliding Mode Controller (HOFOSMC) used to control the frequency and the power shared by the tie-lines of Iraqi three areas interconnected power system model. The proposed controller is analysed under various load disturbances and system parameters uncertainties. Simulation results demonstrate, under a 15% ramp load disturbance, HOFOSMC reduces the maximum frequency deviation by up to 60% compared with OFOSMC and approximately 83% compared with OSMC, while also shortening the settling time by 60% and 83%, respectively. Furthermore, under stochastic white-noise disturbances, HOFOSMC achieves reductions of up to 33% and 56% in peak frequency deviations, along with corresponding reductions in settling time, relative to OFOSMC and OSMC. These results confirm the superior robustness, faster damping, and enhanced stability of the proposed HOFOSMC for LFC of the Iraqi three-area interconnected power system.

1. Introduction

Load Frequency Control (LFC) is a secondary control system responsible for stabilize the performance of the active power in reaction to changes in generation and consumer uses, which otherwise cause deviations from the nominal system frequency and compromise power system

stability and resilience [1]-[6]. Due to this problem, LFC plays crucial role in keeping power system frequency stable and robust under disturbances and maintaining regular power exchange among interconnected areas [7]-[12]. In addition to uncertainties in system characteristics, the variable output power of renewable generators and unpredictable load variations contribute to uncertainties in power system, potentially leading to significant frequency deviations [13]-[18]. The researchers used a number of control strategies to solve the issue of frequency fluctuations. Various control procedures have been proposed in the LFC field, including classical control techniques, robust control designs, predictive control methods, intelligent control systems, and adaptive control strategies [19]-[26].

In recent decades, power system have undergone substantial structural and operational transformations owing to advancements in generation technology, energy storage technologies, and the extensive incorporation of renewable energy sources. As a result, contemporary power systems have developed into complex and nonlinear structures, incorporating technologies such as renewable energy sources and superconducting magnetic energy storage [27]. These developments necessitate advanced control approaches capable of effectively handling system nonlinearities, uncertainties, and dynamic operating situations. In real-world power system operation, nonlinear constraints like governor dead-band (GDB) and generation rate constraint (GRC) are very important to ensure best performance of the power system. The governor dead-band (GDB) is the part of the governor mechanism that causes the system to respond more slowly. The generation rate constraint (GRC), on the other hand, is the physical limit on how quickly the output of a generator can change. This makes it hard to quickly shift the power during disruptions.

In such complex and nonlinear power system, frequency becomes a critical parameter of power system that requires constant monitoring and regulation to guarantee safe, stable, and reliable operation. However, traditional control solutions are often successful only at specific operating points and frequently struggle to deal with large-scale interconnected power system with nonlinear behaviour and parametric uncertainties. Consequently, alternative strategies of LFC, such as evolutionary computation-based controllers, intelligent control methods, and state feedback control systems, have been extensively studied [28]. A detailed review on LFC control systems has been provided, outlining their respective merits and disadvantages.

Classical controllers, such as PI and PID, are used in areas 1 and 2 of the micro-grid to improve frequency and power stability [29]-[36]. Furthermore, numerous optimization methods have been developed for an ideal LFC framework [37]-[39]. Nonetheless, the created controllers do not have extraordinary settling times, peak overshoot, or peak undershoots values. The classical controllers are implemented commonly in LFC fields; however their response suffer from error steady state under nonlinearities, and disturbances. Alternatively, the Integral tilt-integral-derivative with filter (I-TDN) controller was initially implemented to evaluate the performance of load frequency control (LFC) in interconnected multi-source power system (MSPS) [40]. A complete multivariable Model Predictive Control (MPC) is designed to address load frequency control (LFC) in a multi-area power system. The proposed control technique aims to meet LFC's multivariable feature s, system uncertainty, and generation rate limits all at the same time [41]-[46]; however its high computational burden effect on its practical applicability in large scale power system.

The Sliding Mode Controller (SMC) is widely used in frequency control difficulties for integrated power system with uncertainties and model imperfections [47]-[54]. SMC is well-known for its robustness; nevertheless, excessive chattering remain major drawbacks. Fractional-order (FO) controllers have recently gained a lot of attention for resolving frequency instability in power system because of its design flexibility and control effectiveness [55]-[57]. In spite of its tuning flexibility but it is still have practical implementation complexity and sensitive to parameter selection.

This study analyses a three areas Iraqi power system using real data provided by Iraq's Ministry of Electricity [58], encompassing the northern, central, and southern regions, which contain variety generation sources such as hydroelectric, gas, diesel, and thermal units. To enhance frequency regulation performance, an improved Hybrid Optimized Fractional Order Sliding Mode Controller

(HOFOSMC) is designed and integrated into the model with ant Colony Optimization (ACO) employed to improve the controller's performance. The research contributions of this work are:

1. In contrast to standard sliding mode-based LFC techniques, which typically incorporate the integral term within the sliding surface, this study proposes a novel control structure by directly embedding a Proportional-Integral (PI) term into the switching function of the reaching law. This formulation improves disturbance rejection and lowers steady-state error while maintaining the sliding mode controller's inherent resilience, without changing the order or complexity of the sliding surface.
2. This study directly addresses the nonlinearities and realistic operating restrictions prevalent in real-world power system, in contrast to many prior LFC research that depend on simplified system representations. These include Governor Dead Band nonlinearities (GDB) and Generation Rate Constraints (GRC), both of which have a substantial impact on dynamic frequency behaviour. Incorporating these aspects allows for a more realistic evaluation of controller performance and increases the practical applicability of the proposed control method.
3. The suggested control strategy is validated using a sophisticated multi-area model of Iraq's power system, which is structurally complex and has heterogeneous generation units. The confluence of various generation technologies with differing dynamic characteristics presents further issues for frequency management. This study illustrates the efficacy and resilience of the suggested controller under realistic operational settings, hence affirming its appropriateness for extensive interconnected power system.

Together, these contributions advance the theoretical development and practical applicability of fractional order sliding mode control based load frequency control in modern interconnected power system. The flowchart of the research paper shown in Fig. 1.

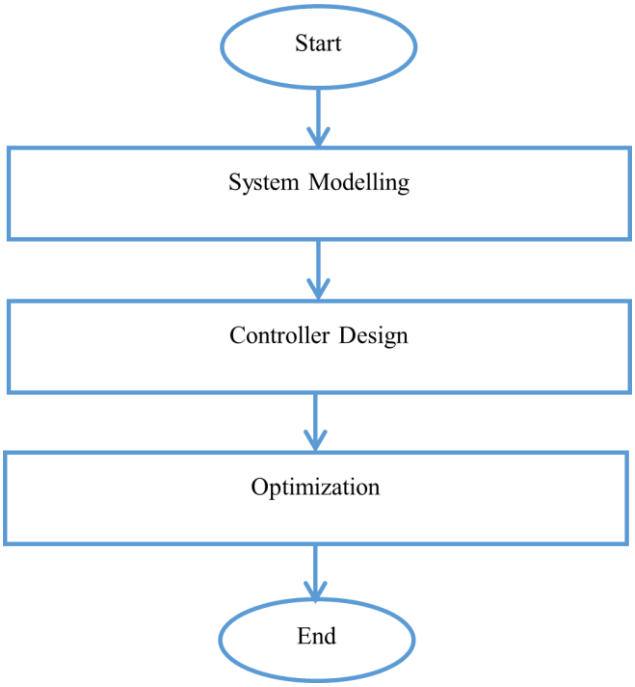

Fig. 1. Flowchart of the proposed research methodology

2. Power System Modeling

The power system utilized is formulated based on basic LFC assumptions, including linearization around a nominal operating point and minimal frequency deviations. During the

analyses, it is assumed some constraints such as Governor Dead Band nonlinearities (GDB), Generation Rate Constraints (GRC) and the power system used is well known simplified model. The Iraqi mathematical model of a power system presented in this research comprises three interconnected control areas, each equipped with its own load frequency controller. The linearized mathematical model for each of the three CAs can be articulated using the following (1):

$$\dot{x}_i(t) = A_i x_i(t) + \sum_j A_{ij} x_j(t) + B_i u_i(t) + F_i d_i(t) + \delta_i(x, u, t) \quad (1)$$

Where x_i is the system state vector, x_j is a state vector of the neighbor's system, u_i is the control signal vector, d_i is the disturbance vector, δ_i is a vector of uncertainties. Matrices (A_i, A_{ij}, B_i, F_i, and δ_i) represents the system state vectors for specific area, the neighbor's system state vectors for other areas, input vector for specific area, disturbance vectors, and uncertainty vectors respectively. The system parameters and network structure used in this study are based on operational data from the Iraqi Ministry of Electricity corresponding to the 2019–2020 period, which represents the most recent complete and consistent dataset available for the national grid [58]. During this period, the Iraqi power system remained predominantly reliant on conventional thermal and gas-turbine generation, and the three-area interconnection structure had not undergone significant structural changes.

2.1. North Area

The northern region of Iraq includes the provinces of Nineveh, Kirkuk, Salah al-Din, and Diyala, and it is distinguished by a varied range of electricity generation sources. This region's installed generation portfolio includes hydroelectric, gas-fired, and diesel power plants, each with its own turbine-governor system, the specifications of which differ by manufacturer. The equivalent system inertia (H_{eq}) was modified proportionally to total installed capacity. The Ministry's official report provides more information on generation capacity and load demand [58]. The inertia for this area was calculated using (2), and the results are provided in Table 1.

$$H_{eq} = \sum_i^N H_i \cdot \frac{S_i}{S_{North}} \quad (2)$$

Table 1. Data generators and system inertia in Iraq's northern region

Generator Unit	Capability of Operation (MW)	$H_i(S)$	$H_{eq}(S.pu.)$
Hydro	187.5	4.5	0.533688
Gas	292	6	2.878445
Diesel	23	0.945	0.055936
Total	502.5	-	3.468

2.2. Central Area

The central area of Iraq includes the cities of Anbar, Baghdad, Najaf, Karbala, Babil, and Diwaniyah. This region utilizes a varied array of power-generation technologies, encompassing hydroelectric, gas-fired, diesel, and thermal facilities. The generation units in the northern and central regions function under identical parameter conditions, as calculated in (3) and provided in Table 2.

2.3. South Area

The southern area of Iraq includes the cities of Basra, Maysan, and Dhi Qar, and is supported by various power-generation facilities, such as thermal, gas-fired, and diesel plants. The identical generation parameter choices utilized for the northern and central areas were likewise implemented in this location, as calculated in (4) and written in Table 3.

$$H_{eq} = \sum_{i}^{N} H_i \cdot \frac{S_i}{S_{Middle}} \quad (3)$$

Table 2. Data Generators and system inertia in Iraq's central region

Generator Type	Capability of Operation (MW)	$H_i(S)$	$H_{eq}(S.pu.)$
Hydro	187.5	4.5	0.15087
Gas	292	6	2.43004
Diesel	23	0.945	0.04111
Thermal	610	6	1.64709
Total	1112.5	-	4.27

$$H_{eq} = \sum_{i}^{N} H_i \cdot \frac{S_i}{S_{South}} \quad (4)$$

Table 3. Data Generators and system inertia in Iraq's south region

Generator Type	Capability of Operation (MW)	$H_i(S)$	$H_{eq}(S.pu.)$
Thermal	610	6	1.51075
Gas	292	6	2.34028
Diesel	23	0.945	0.06868
Total	925	-	3.919

2.4. Iraqi Interconnected Plant

This study implement a simple linked power system model to represent the northern, central, and southern regions of Iraq, aiming to analyses the system's frequency response behaviour, as depicted in Fig. 2. The correlation between load and frequency in each location was consolidated into a singular damping coefficient D, which was given a value of (1 p.u). The governor droop characteristic was modeled using the gain$(1/R)$, assigned a value of 20 per unit across all scenarios. The parameters featured in Fig. 1. are detailed in Table 4, where T_1, T_2, T_r, T_w, T_{gas1}, T_{gas2}, T_{d1}, T_{d2}, T_{th1}, T_{th2} represent the time constants of the turbine-generator units. Additionally, the frequency bias coefficient (B) was set to 21 per unit, as defined by (5).

$$B = \frac{1}{R} + D \quad (5)$$

A multi-area power system describes regions that are linked by high-voltage transmission lines. Besides maintaining frequency stability in each region, the controller in every control area is responsible for managing power flow across the tie-lines, minimizing deviations between neighboring regions, and reducing the area control errors (ACE_1, ACE_2, and ACE_3). The expected net power exchange among the northern, central, and southern regions of Iraq is detailed in equations (6) to (8).

The coefficients (K_{12},K_{21},K_{13},K_{31},K_{23}, andK_{32}) denote the synchronizing torque constants between interconnected zones Table 5. The symbols (Δf_1,Δf_2,Δf_3) refer to the frequency deviations in the northern, central, and southern regions, respectively. To ensure frequency coherence among the zones and along the interconnected paths, the area control error ACE_i must be minimized to zero promptly, while also keeping chattering effects to a minimum. The corresponding ACE_i formulations are provided in equations (9), (10), and (11).

$$\Delta P_{tie,12} = \frac{2\pi}{S} . K_{12} . \left(\Delta f_1(s) - \Delta f_2(s)\right) \quad (6)$$

$$\Delta P_{tie,13} = \frac{2\pi}{S}.K_{13}.\left(\Delta f_1(s) - \Delta f_3(s)\right) \quad (7)$$

$$\Delta P_{tie,23} = \frac{2\pi}{S}.K_{23}.\left(\Delta f_2(s) - \Delta f_3(s)\right) \quad (8)$$

Table 4. Generators and system model parameters

R	B	T_1	T_2	T_r	T_w	T_{gas1}	T_{gas2}	T_{d1}	T_{d2}	T_{th1}	T_{th2}
0.05	21	0.2	38	5	1	0.3	0.2	0.2	0.05	0.3	0.08

Table 5. Interconnection tie-line parameters

K_{12}	K_{21}	K_{13}	K_{31}	K_{23}	K_{32}
0.05	21	0.2	38	5	1

$$\text{For north area } ACE_1(t) = -(2.\pi.K_{12}.(\Delta f_1 - \Delta f_2) + 2.\pi.K_{13}.(\Delta f_1 - \Delta f_3) + B_1.\Delta f_1) \quad (9)$$

$$\text{For middle area } ACE_2(t) = -(2.\pi.K_{12}.(\Delta f_2 - \Delta f_1) + 2.\pi.K_{23}.(\Delta f_2 - \Delta f_3) + B_2.\Delta f_2) \quad (10)$$

$$\text{For south area } ACE_3(t) = -(2.\pi.K_{13}.(\Delta f_3 - \Delta f_1) + 2.\pi.K_{23}.(\Delta f_3 - \Delta f_2) + B_3.\Delta f_3) \quad (11)$$

3. Design and implementation of the Hybrid Optimized Fractional Order Sliding Mode Controller (HOFOSMC)

This section discusses the Hybrid Optimized Fractional Order Sliding Mode Controller (HOFOSMC). The FOSMC fails often to mitigate steady-state error response. Therefore, HOFOSMC has been designed using the same methodology as fractional order sliding mode control. However, it differs by incorporating a proportional-integral sat (PI) term directly into the reaching laws (u_{eq1},u_{eq2},u_{eq3}), alongside the conventional switching term ($tan^{-1}(S_i/\emptyset)$) to mitigate steady-state error response. In this work, the sliding surface $S_i(t)$ has been selected for each area; north, middle, and south respectively as depicted in (12)-(14):

$$S_{north} = c_1.ACE_1 + c_{11}.D^{\alpha}(ACE_1) \quad (12)$$

$$S_{central} = c_2.ACE_2 + c_{22}.D^{\alpha}(ACE_2) \quad (13)$$

$$S_{south} = c_3.ACE_3 + c_{33}.D^{\alpha}(ACE_3) \quad (14)$$

In this context, ACE_1, ACE_2, and ACE_3 denotes the tracking error for each area, while c_1, c_{11}, c_2, c_{22} , c_3, c_{33} are positive control parameters determined by the designer and (D^{α}) is the fractional derivative of order (α) which is typically between zero and one. The primary objective of the control strategy is to driveACE_1,ACE_2 and ACE_3 and its derivatives to zero at all times once the sliding surfacesS_{north},S_{middle} S_{south} are reached. Consequently, maintaining a constant value of $S_i(t)$ requires that its time derivative be zero, which is mathematically expressed as (15):

$$\dot{S}_i(t) = 0 \quad (15)$$

The fractional order sliding mode control law $u_{eqi}(t)$ is composed of two components: a nominal component $u_{ci}(t)$ and a switching component $u_{h-switch}$, as described in (16):

$$u_{eqi}(t) = u_{ci}(t) + u_{h-switch}(t) \quad (16)$$

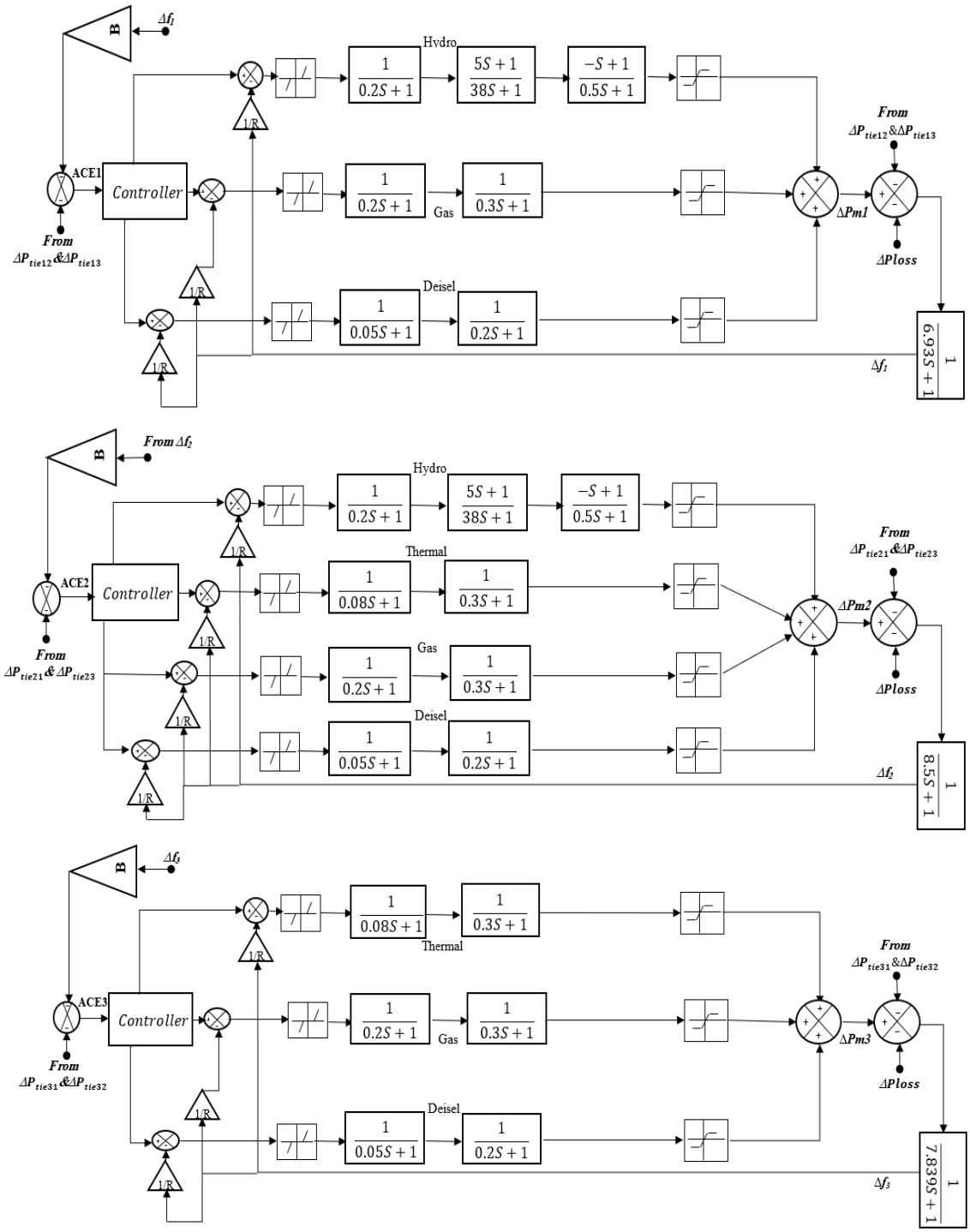

Fig. 2. Block diagram of Iraqi interconnected model

The model has been considered and has been written in differential form in each area. The derivation of the sliding surface $\dot{S}_i$ can be simplified for three areas north, middle, and south after substituting the area control error ACE_1, ACE_2, and ACE_3. We substitute the differential equations of$\dot{x}_1$,$\dot{x}_{10}$, and $\dot{x}_{21}$ which are represent the Δf_1, Δf_2, and Δf_3 respectively. Thus, the resulting sliding mode controller's $u_{eqi}(t)$ for each area are presented as follows (17)-(19):

$$u_{eq1}(t) = u_{c1} + u_{h-switch} \tag{17}$$

$$u_{eq2}(t) = u_{c2} + u_{h-switch} \tag{18}$$

$$u_{eq3}(t) = u_{c3} + u_{h-switch} \tag{19}$$

In this study, the hybrid fractional order sliding mode controller is modified by including two switching functions; conventional switching and PI switching to mitigate the chatter and the steady state error. The $u_{h-switch}$ term includes the conventional switching and the PI switching is presented as follows (20)-(22):

$$u_{eq1}(t) = u_{c1} - k_1.tan^{-1}(S_1/\emptyset) - k_{11}\int sat\left(\frac{S_1}{\emptyset}\right).dt \tag{20}$$

$$u_{eq2}(t) = u_{c2} - k_2.tan^{-1}(S_2/\emptyset) - k_{22}\int sat\left(\frac{S_2}{\emptyset}\right).dt \tag{21}$$

$$u_{eq3}(t) = u_{c3} - k_3.tan^{-1}(S_3/\emptyset) - k_{33}\int sat\left(\frac{S_3}{\emptyset}\right).dt \tag{22}$$

Here, $tan^{-1}\frac{S_i}{\emptyset}$ is included in the controller to establish the boundary layer of the control law. The tuning parameters (k_1, k_2, k_3, k_{11}, k_{22}, k_{33}, c_1, c_{11}, c_2, c_{22}, c_3, c_{33}, α and $\emptyset$) are obtained with the use of the metaheuristic optimization techniques. The Ant Colony Optimization (ACO) technique used in this research to obtain the optimal controller parameters in equations. The Integral Square Error signal (ITSE) is taken as objective function for each area as (23):

$$ITSE = \int e(t)^2.dt \tag{23}$$

3.1. Lyapunov Stability Proof

For each control area the sliding surface is denoted $S_i(t)$:

$$V_i(t) = \frac{1}{2}(S_i)^2 \tag{24}$$

$$\dot{V}_i(t) = S_i\dot{S}_i \tag{25}$$

$$u_{eq(i)} = u_{c(i)} + u_{h-switch} \tag{26}$$

$$u_{h-switch} = -k_i\ tan^{-1}(S_i/\emptyset) - k_{ii}\int_0^t sat\left(\frac{S_i}{\emptyset}\right)dt \tag{27}$$

Where $(k_i, k_{ii} > 0)$. After substituting the closed loop dynamics, the time derivative of sliding surface can be written in the compact form:

$$S_i = \mu_i(t) - k_i\tan^{-1}\left(\frac{S_i}{\emptyset}\right) - k_{ii}\gamma_i \tag{28}$$

$$\gamma_i = \int_0^t sat(\frac{S_i}{\emptyset})\ dt \tag{29}$$

Where $\mu_i(t)$ represent the lumped matched uncertainties and disturbances. It is assumed $\mu_i(t)$ is bounded such that:

$$|\mu_i(t)| \leq \bar{\mu_i} \tag{30}$$

Then, Lyapunov derivative become:

$$\dot{V}_i(t) = S_i\mu_i(t) - k_i S_i \tan^{-1}\frac{S_i}{\emptyset} - k_{ii}S_i\gamma_i \tag{31}$$

Using inequality:

$$|S_i\mu_i| \leq \bar{\mu_i}|S_i| \tag{32}$$

And noting that: $S_i \tan^{-1}\frac{S_i}{\emptyset} > 0$, for $S_i \neq 0$. We obtain:

$$\dot{V}_i(t) \leq -(k_i - \bar{\mu_i})|S_i| - k_{ii}S_i\gamma_i \tag{33}$$

By selecting control gain such as $(k_i > \bar{\mu_i})$. It follows that $\dot{V}_i(t) < 0$, $\forall S_i \neq 0$ which guarantee the reaching condition $S_i\dot{S}_i < 0$. Here, sliding surface $S_i(t)$ is globally attractive and closed loop system converge towards sliding manifold. The additional PI switching term $(-K_{ii}\int \text{sat}(\frac{S_i}{\emptyset})\ dt)$ ensuring convergence, eliminating steady state error, and chattering reduction.

4. Optimization Technique

Metaheuristic optimization techniques offer effective and cost-efficient methods for tuning fractional controllers. These strategies rely on an objective function to assess solution performance and determine the optimal parameter values [59], [60]. This study employs the Ant Colony Optimization (ACO) algorithm to optimize fourteen parameters of the HOFOSMC controller and an additional eleven parameters of the optimized fractional order (OFOSMC) controller, aiming to enhance system response. In load frequency control of interconnected power system, ACO is well suited to this environment, as its probabilistic search and pheromone-updating mechanism effectively balance exploration and exploitation, enabling reliable convergence toward high-quality solutions without being trapped in local minima. The cost function presented in (34) is utilized to minimize the Area Control Error (ACE_i) aiming for a zero error in each area by aggregating the squared area control errors for three areasACE_1, ACE_2, and ACE_3, multiplied by time (t). The parameter bounds and converge criteria are illustrated in Table 6.

$$\text{Cost value} = \int_0^\infty (t.\,\text{ACE}_1{}^2 dt + t.\,\text{ACE}_2{}^2 dt + t.\,\text{ACE}_3{}^2 dt) \tag{34}$$

Table 6. ACO parameters through all cases

Method	Value
Number of Ants	100
Alpha	0.8
Beta	0.2
Evaporation rate	0.7
Initial pheromone	0.01
Max Iterations	100

5. Simulation Results and Discussion

This section presents a comprehensive simulation analysis to validate the performance of the proposed HOFOSMC control scheme, utilizing a benchmark power system model presented in Fig. 1. This dynamic model incorporates parameter variability, modelling inaccuracies, aggregated disturbances from load and generation fluctuations, nonlinearities (GDB & GRC), conventional generation. However, this study focuses on three-area system interconnected by tie-lines. A comprehensive power system model is constructed utilizing MATLAB software version 2019b to

simulate a genuine system for the evaluation of the designed controller. The analysis of the current work's performance is undertaken under several test scenarios taking into account diverse disturbance instances and operating settings to replicate the actual power system. The simulation study is performed to examine the dynamic performance of interconnected power system. The simulation results are presented and analysed as follows.

5.1. Scenario 1

A simulation analysis is performed in such a scenario, concentrating on the ramp disturbance (15%) from t = 10 seconds to t = 16 seconds, particularly within area 1, as specified in Table 7. The system's overall performance is assessed, and the corresponding frequency variation for each area is illustrated in Fig. 3, Fig. 4, Fig. 5.

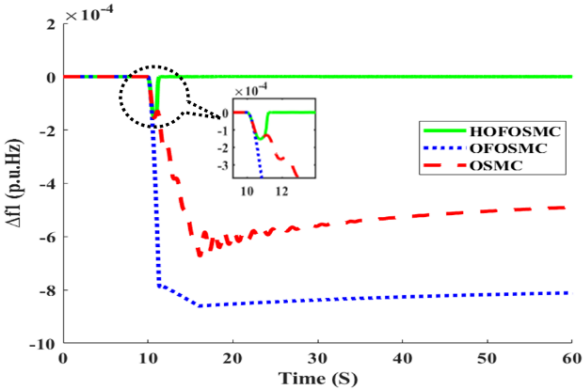

Fig. 3. Frequency regulation (Δf1) of area 1 scenario 1

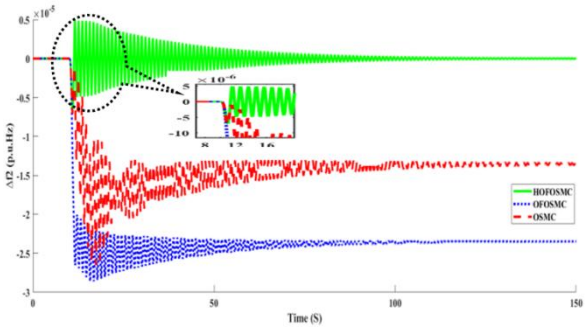

Fig. 4. Frequency regulation (Δf2) of area 2 scenario 1

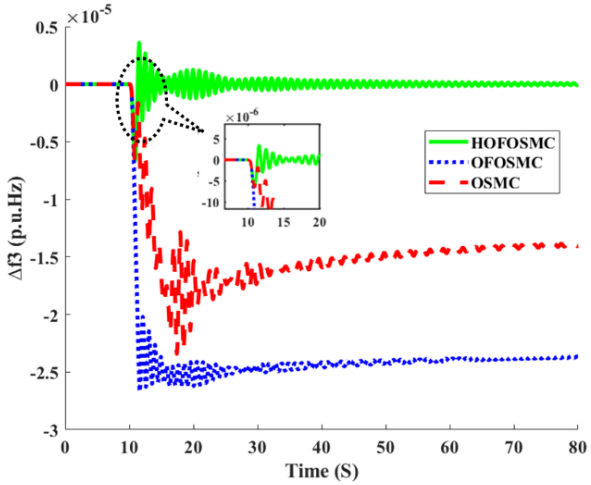

Fig. 5. Frequency regulation (Δf3) of area 3 scenario 1

Table 7. Simulation values of three-areas with 15% ramp disturbance in area 1 only

Controller	Peak value (p.u. Hz)	Settling time $t_s(S)$	$Absolute\ E_{s.s}$	Area
HOFOSMC	$-0.9 * 10^{-4}$	12	$5.7 * 10^{-8}$	1
OFOSMC	$-8.6 * 10^{-4}$	30	$7.9 * 10^{-4}$	1
OSMC	$-6.7\ x\ 10^{-4}$	70	$4.6\ x\ 10^{-4}$	1
HOFOSMC	$-0.47\ x\ 10^{-5}$	110	0	2
OFOSMC	$-2.62\ x\ 10^{-5}$	70	$2.35\ x\ 10^{-5}$	2
OSMC	$-2.85\ x\ 10^{-5}$	120	$1.35\ x\ 10^{-5}$	2
HOFOSMC	$-0.61\ x\ 10^{-5}$	45	0	3
OFOSMC	$-2.61\ x\ 10^{-5}$	30	$2.35\ x\ 10^{-5}$	3
OSMC	$-2.29\ x\ 10^{-5}$	55	$1.4\ x\ 10^{-5}$	3

Under ramp disturbances, HOFOSMC exhibits superior performance by achieving the shortest settling time, minimal overshoot, and zero steady-state error compared with OSMC and OFOSMC. This scenario examines the dynamic performance of a three-area interconnected power system under a 15% ramp load disturbance applied just to area 1. The frequency responses of regions 1, 2, and 3 (Fig. 3, Fig. 4, Fig. 5) show that the disturbance in area 1 propagates to surrounding regions via tie-line coupling, resulting in considerable frequency deviations in areas 2 and 3. The comparison results show a clear performance hierarchy among the controllers. The suggested HOFOSMC consistently has the smallest peak deviations and the fastest convergence in all domains. Specifically, area 1 has a settling time of about 12seconds with HOFOSMC, compared to 30seconds and 70seconds for OFOSMC and OSMC, respectively, demonstrating a significant improvement in disturbance rejection capability. Similar patterns are observed in areas 2 and 3, where HOFOSMC reaches settling periods of 110seconds and 45seconds, whereas OSMC requires up to 120seconds and 55seconds, respectively. The fractional dynamics add degrees of freedom to dampen low-frequency inter-area oscillations, whilst the integral term compensates for the accumulated error caused by the ramp disturbance, reducing steady-state bias.

5.2. Scenario 2

The proposed Hybrid-Order Fractional Sliding-Mode Controller (HOFOSMC) is tested for robustness against noise. The noise is modelled as band-limited white noise injected into area 3 at time t = 20seconds. White-noise excitation depicts actual random variations caused by load unpredictability, and renewable penetration according to Table 8. The system's overall performance is assessed, and the corresponding frequency variation for each area is illustrated in Fig. 6, Fig. 7, Fig. 8.

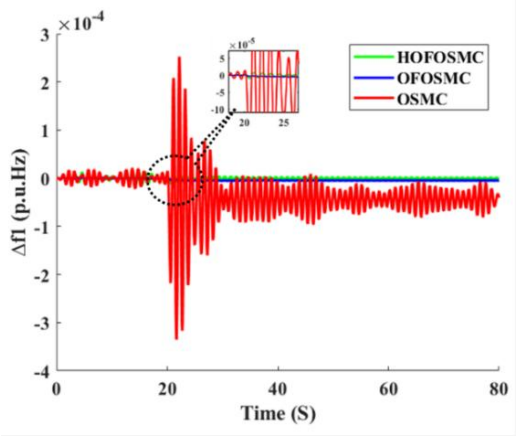

Fig. 6. Frequency regulation (Δf1) of area 1 scenario 2

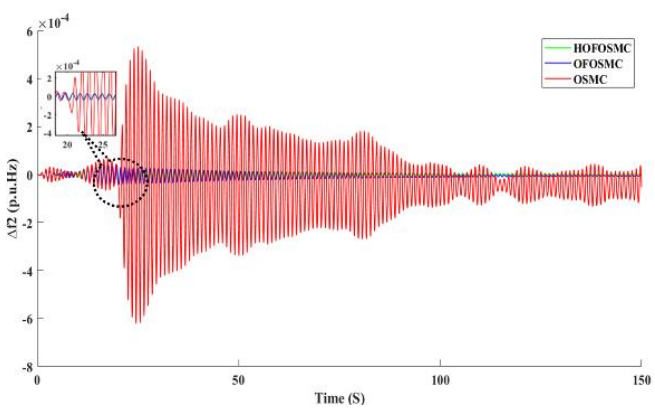

Fig. 7. Frequency regulation (Δf2) of area 2 scenario 2

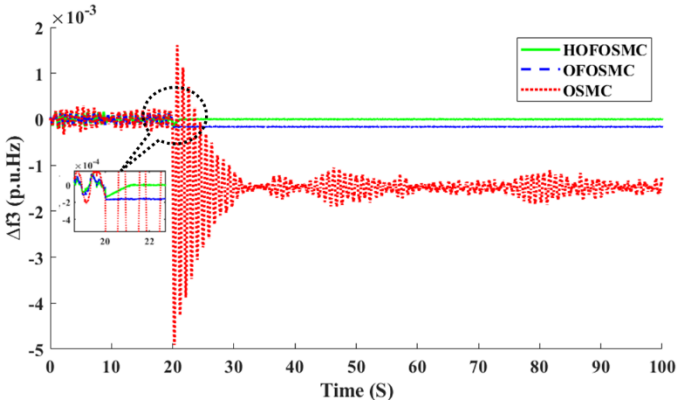

Fig. 8. Frequency regulation (Δf3) of area 3 scenario 2

Table 8. Simulation values of three-areas with white noise in area 3 only

Controller	Peak value (p.u. Hz)	Settling time $t_s(S)$	$Absolute\ E_{s.s}$	Area
HOFOSMC	$-0.6\ x\ 10^{-4}$	25	0	1
OFOSMC	$-2.7\ x\ 10^{-4}$	35	$1.5\ x\ 10^{-4}$	1
OSMC	$-3.5\ x\ 10^{-4}$	50	$2.5\ x\ 10^{-4}$	1
HOFOSMC	$-1.4\ x\ 10^{-4}$	40	0	2
OFOSMC	$-2.3\ x\ 10^{-4}$	60	$2.3\ x\ 10^{-4}$	2
OSMC	$-7.2\ x\ 10^{-4}$	100	$1.3\ x\ 10^{-4}$	2
HOFOSMC	$-2\ x\ 10^{-4}$	40	$1\ x\ 10^{-4}$	3
OFOSMC	$-3\ x\ 10^{-4}$	60	$2\ x\ 10^{-4}$	3
OSMC	$-5\ x\ 10^{-3}$	90	$2\ x\ 10^{-3}$	3

Under white noise, HOFOSMC exhibits superior performance by achieving the shortest settling time, minimal overshoot, and zero steady-state error compared with OSMC and OFOSMC. According to Fig. 6, the suggested HOFOSMC has the lowest peak deviation and fastest attenuation following noise excitation. The response settles to a tiny random band around zero within 25seconds, while OFOSMC and OSMC take 35seconds and 50seconds respectively. area 1 under HOFOSMC has almost no steady-state bias, whereas OFOSMC and OSMC have detectable offsets of order $10^{-4}p.u.Hz$. A similar trend is observed in Fig. 7. Although area 2 does not directly receive the noise input, it experiences considerable oscillations under OSMC, with high-amplitude residual oscillations persisting beyond 100seconds. By comparison, HOFOSMC reduces the peak deviation by roughly (40%-80% *p.u. Hz)* relative to the compared controllers and settles in about 40seconds, whereas OFOSMC requires 60seconds and OSMC effectively does not reach a stable bounded response within the simulated horizon. As expected, the highest disturbance occurs in area 3 Fig. 8, where the noise is injected. OSMC shows large transient spikes of $10^{-3}p.u.Hz$ and a slow-decaying oscillatory envelope. In comparison, HOFOSMC restricts peak deviation by nearly an order of magnitude and converges to a tight stationary noise band within 40seconds, whereas other controllers require more than 60seconds or fail to settle during the observation period.

5.3. Scenario 3

This scenario investigates controller robustness when two important system parameters are deliberately disrupted. The frequency bias factor (B) at time 20seconds at area 1 changes by (±20%) and the governor drops (R) in area 3 at time 25seconds. Meanwhile, a (15%) step load disruption is applied just to area 2. This coupled disturbance-uncertainty situation is thus one of the most demanding robustness tests in multi-area LFC are shown in Fig. 9, Fig. 10, Fig. 11, Fig. 12, Fig. 13, Fig. 14.

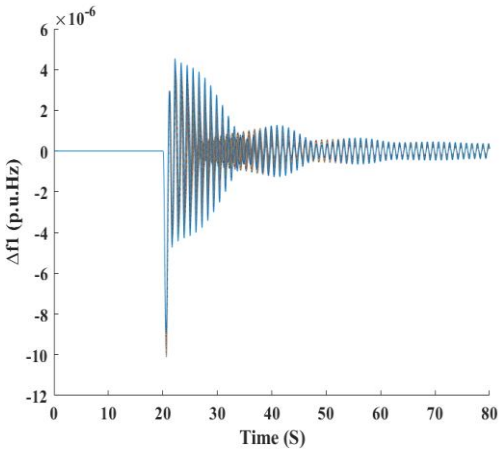

Fig. 9. Frequency regulation (Δf1) of area 1 scenario 3 with uncertainties (B=±20%) using HOFOSMC

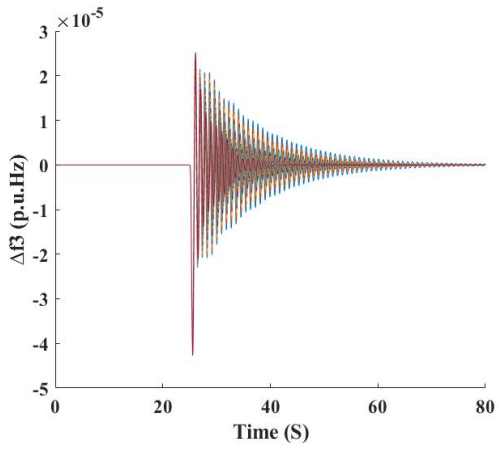

Fig. 10. Frequency regulation (Δf3) of area 3 scenario 3 with uncertainties (R=±20%) using HOFOSMC

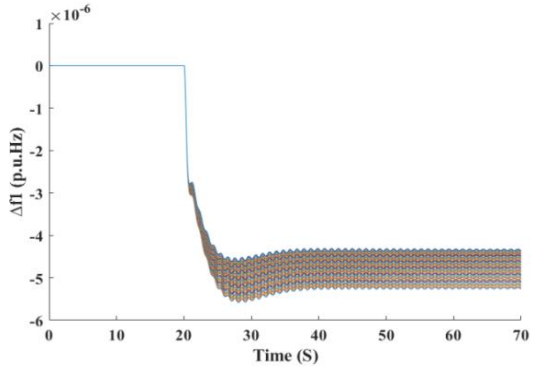

Fig. 11. Frequency regulation (Δf1) of area 1 scenario 3 with uncertainties (B=±20%) using OFOSMC

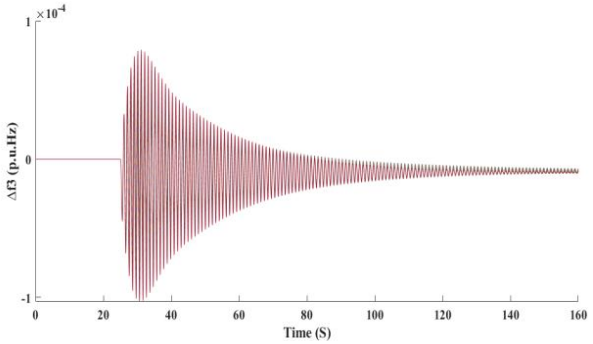

Fig. 12. Frequency regulation (Δf3) of area 3 scenario 3 with uncertainties (R=±20%) using OFOSMC

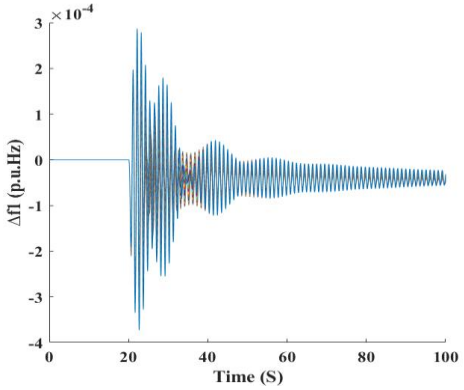

Fig. 13. Frequency regulation (Δf1) of area 1 scenario 3 with uncertainties (B=±20%) using OSMC

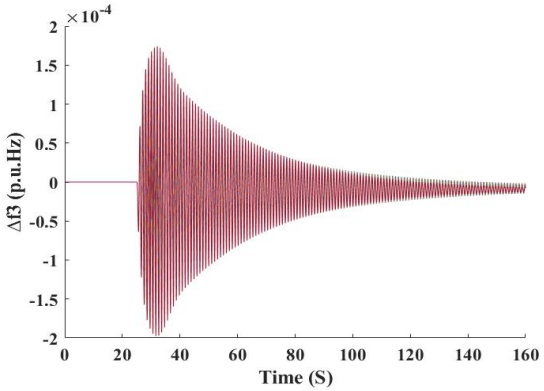

Fig. 14. Frequency regulation (Δf3) of area 3 scenario 3 with uncertainties (R=±20%) using OSMC

HOFOSMC Fig. 9 maintains very small deviations and quick recovery despite ±20% disturbance in (B). The curve remains tightly confined and approaches zero, suggesting that the sliding manifold is still intact even when the bias-factor mismatch occurs. OFOSMC Fig. 11 has stronger oscillations and a visible steady-state offset, indicating that the fractional-order surface alone is insufficient to completely reject structural uncertainty. OSMC Fig. 13 has the widest oscillation envelope and slowest decline; with much more overshoot than the fractional-order instances. This reflects traditional SMC's significant sensitivity to modelling errors, particularly when no integral-type compensation is used. Overall, HOFOSMC shows superior robustness by maintaining frequency stability in the bias-perturbed area even when the disturbance occurs remotely at area 2. Under HOFOSMC Fig. 10, the response is bounded and well-damped with only minor transient excursions after a ±20% change in (R). Despite the parameter discrepancy, the system quickly returns to the sliding area, demonstrating high invariance features. OFOSMC Fig. 12 exhibits larger oscillations and slower convergence as the droop uncertainty alters the sliding controller's effective control gain. OSMC Fig. 14 reacts forcefully, generating strong transient spikes and prolonged oscillations particularly immediately following the droop perturbation. This indicates that conventional SMC is not robust to multiplicative uncertainty in the control channel, resulting in poor damping and excessive chattering-like oscillations. Table 9 is illustrated a comparative study with previous works of different controllers on interconnected power system.

The main finding in this paper that the superior performance of the proposed HOFOSMC can be attributed to several structural features. The fractional-order sliding surface introduces memory effects that enhance damping and improve transient behaviour under load disturbances. In addition, the integral action embedded in the control law ensures complete elimination of steady-state

frequency deviations. The hybrid optimized reaching law further accelerates convergence while mitigating chattering, thereby improving robustness against parameter uncertainties and nonlinearities.

Compared with existing ISMC and FOSMC based approaches reported in the literature, where integral action is typically embedded within the sliding surface, the proposed HOFOSMC introduces the integral term directly into the reaching law using a PI-based structure. As summarized in Table 9, this structural distinction enables the proposed controller to achieve lower peak frequency deviations under comparable or more severe disturbance conditions, particularly in multi-area power systems with nonlinearities and uncertainties.

The improved performance of HOFOSMC can be attributed to its structural characteristics. The fractional-order sliding surface introduces memory effects that enhance damping and improve transient behavior. Meanwhile, the PI-based reaching law ensures fast convergence and eliminates steady-state frequency error without excessive integral windup. In addition, the sliding-mode framework provides strong robustness against system uncertainties, nonlinearities, and stochastic disturbances.

The main strengths of this study include the use of a realistic three-area power system model, comprehensive disturbance scenarios, and explicit consideration of nonlinearities and uncertainties. However, the present work is limited to simulation-based validation, and real-time implementation of fractional-order operators on SCADA/PLC hardware has not been addressed. These aspects represent important directions for future research.

Table 9. Comparison of reported and proposed work for multi-area power systems

Author	Multi-Area Considered	Type of Controller	Optimization Algorithm	Tie-Line	Nonlinearity (GDB, GRC)		Disturbance (p.u.)	$peak\ \Delta f(p.u.)$
[21]	1		PID	GA, DE, PSO	No	No	0.01	$-6.4\ x\ 10^{-3}$
[20]	2		PID, PI, I	No	Yes	No	0.02	$-7.9\ x\ 10^{-3}$
[22]	2		FOPID	Firefly	Yes	No	0.01	$-2.0\ x\ 10^{-3}$
[27]	2		FOPID	MPA	Yes	No	0.05	$-0.73\ x\ 10^{-5}$
[28]	2		FOPID, FOTID	SSA	Yes	Yes	0.01	-0.15
[32]	2		SMC	Lyapunov	Yes	No	0.05	-0.02
[33]	2		Super twisting SMC	Adaptive Fuzzy	Yes	Yes	Random	$-5\ x\ 10^{-4}(\Delta f1)$ $-2\ x\ 10^{-4}(\Delta f2)$
[34]	2, 3,4		SMC	PSO, GWO	Yes	Yes	0.1SD	$-0.35\ x\ 10^{-4}$
[37]	3		ISMC	No	Yes	No	0.1SD	-0.038
[39]	2		TSMC	Adaptive	Yes	No	Random	-0.4695 (Δf1) -0.6086 (Δf2)
[40]	2		ISMC	PSO	Yes	No	Random	$-0.7\ x\ 10^{-3}(\Delta f1)$ $-0.8\ x\ 10^{-3}(\Delta f2)$
Proposed Work	3		OSMC, OFOSMC, HOFOSMC	ACO	Yes	Yes	SD (15%), Ramp disturbance	$-0.6\ x\ 10^{-4}(\Delta f1)$ $-0.47\ x\ 10^{-5}(\Delta f2)$ $-0.61\ x\ 10^{-5}(\Delta f3)$

P: Proportional, I: Integral, D: Derivative, FO: Fractional Order, SMC: Sliding Mode Controller, GA: Genetic Algorithm, PSO: Particle Swarm Optimization, GWO: Grey-Wolf Optimization, ACO: Ant-Colony Optimization, SD: Step disturbance, Δf: Frequency Deviation

6. Conclusion

This study detailed the design and performance assessment of three sophisticated nonlinear secondary frequency controllers Optimized Sliding Mode Control (OSMC), Optimized Fractional-Order Sliding Mode Control (OFOSMC), and a Hybrid Optimized Fractional-Order Sliding Mode Controller (HOFOSMC) utilizing a PI-based reaching law implemented in a realistic three areas Iraqi interconnected power system featuring hydro, thermal, gas, and diesel generation units. The

controllers were tested in real-world situations, such as ramp load disturbances, random white noise excitation, and ±20% changes in frequency bias and governor droop, as well as external load disturbances.

The simulation findings show that HOFOSMC always does better than OSMC and OFOSMC when it comes to transient response, resilience, and steady-state accuracy. When there are ramp load disturbances, HOFOSMC has the lowest peak frequency deviation and the fastest settling time in all areas. It also completely gets rid of steady-state error. On the other hand, OSMC and OFOSMC show larger oscillations and steady-state biases that last throughout interconnected disturbance propagation. When there is white noise, HOFOSMC does a better job of reducing noise by (40-80%) and limiting frequency variations to a narrow band around the nominal value.

Robustness investigation with parameter changes of ±20% shows again that HOFOSMC has robust and well-damped dynamics with little overshoot and quick convergence. These gains come from the combination of fractional-order dynamics, which add memory features that make damping and robustness better, and the PI-based reaching rule, which makes sure that convergence is quick and there is no steady-state error. In general, HOFOSMC is a realistic and strong way to regulate frequency that combines the standard reliability of SMC with the improved performance of fractional-order dynamics.

Future work will examine the real-time reliability of fractional-order operators on SCADA/PLC hardware, including challenges related to discretization accuracy, computational complexity, and hardware constraints.

Author Contribution: All authors contributed equally to the main contributor to this paper. All authors read and approved the final paper.

Funding: This research received no external funding.

Conflicts of Interest: The authors declare no conflict of interest.

References

[1] H. H. Alhelou, M. E. H. Golshan, and P. Siano, "Frequency response models and control in smart power systems with high penetration of renewable energy sources," *Computers & Electrical Engineering*, vol. 96, p. 107477, 2021, https://doi.org/10.1016/j.compeleceng.2021.107477.

[2] M. Dashtdar *et al*., "Frequency control of the islanded microgrid based on optimised model predictive control by PSO," *IET Renewable Power Generation*, vol. 16, no. 10, pp. 2088-2100, 2022, https://doi.org/10.1049/rpg2.12492.

[3] S. Ke *et al*., "A Frequency Control Strategy for EV Stations Based on MPC-VSG in Islanded Microgrids," *IEEE Transactions on Industrial Informatics*, vol. 20, no. 2, pp. 1819-1831, 2024, https://doi.org/10.1109/TII.2023.3281658.

[4] S. Ramnarain and K. Reddy, "A comprehensive review of load frequency control of decentralized networks," *2025 33rd Southern African Universities Power Engineering Conference (SAUPEC)*, pp. 1-6, 2025, https://doi.org/10.1109/SAUPEC65723.2025.10944395.

[5] J. Hussain, R. Zou, Z. Wu, P. K. Pathak, and S. Akhtar, "Design and Performance Analysis of Walrus Optimization Algorithm (WaOA)-Based Cascade Controller for Load Frequency Control of a Multi-Area Power System With Renewable Sources," *International Journal of Numerical Modelling: Electronic Networks, Devices and Fields*, vol. 38, no. 2, p. e70046, 2025, https://doi.org/10.1002/jnm.70046.

[6] G. Ahmad, N. M. Al-Yazidi, M. Shafiullah and M. M. Hamdan, "Metaheuristic-Based Load Frequency Control for EVs-Integrated Hybrid Power Systems with Delays," *2025 IEEE 22nd International Multi-Conference on Systems, Signals & Devices (SSD)*, pp. 922-927, 2025, https://doi.org/10.1109/SSD64182.2025.10989875.

[7] H. Li, X. Wang and J. Xiao, "Adaptive Event-Triggered Load Frequency Control for Interconnected Microgrids by Observer-Based Sliding Mode Control," *IEEE Access*, vol. 7, pp. 68271-68280, 2019, https://doi.org/10.1109/ACCESS.2019.2915954.

[8] E. Thajeel, "An optimal area power system-based automatic load frequency control using a 1-D lookup table method," *Engineering and Technology Journal*, vol. 43, no. 8, pp. 659-669, 2025, https://doi.org/10.30684/etj.2025.156707.1888.

[9] F. J. Zwayyer, A. A. Abbood, and J. F. Hussein, "Optimization of Automatic Generation Control and Economic Load Dispatch for Two Area Six Unit Interconnected Power System," *Engineering and Technology Journal*, vol. 39, no. 10, pp. 1610-1624, 2021, https://web.archive.org/web/20220116144655id_/https://etj.uotechnology.edu.iq/article_169843_ee7ce949dfe198c2d36cd06cf5aa3945.pdf.

[10] M. T. Muhssin, Z. A. Obaid, K. Al-Anbarri, L. M. Cipcigan, and M. N. Ajaweed, "Local dynamic frequency response using domestic electric vehicles," *International Journal of Electrical Power & Energy Systems*, vol. 130, p. 106920, 2021, https://doi.org/10.1016/j.ijepes.2021.106920.

[11] H. Wang and Z. S. Li, "Multi-Area Load Frequency Control in Power System Integrated With Wind Farms Using Fuzzy Generalized Predictive Control Method," *IEEE Transactions on Reliability*, vol. 72, no. 2, pp. 737-747, 2023, https://doi.org/10.1109/TR.2022.3177045.

[12] A. Singh, S. Yadav, N. Tiwari, D. K. Nishad, and S. Khalid, "Optimized PID controller and model order reduction of reheated turbine for load frequency control using teaching learning-based optimization," *Scientific Reports*, vol. 15, no. 1, p. 3759, 2025, https://doi.org/10.1038/s41598-025-87866-z.

[13] F. Farivar, O. Bass and D. Habibi, "Decentralized Disturbance Observer-Based Sliding Mode Load Frequency Control in Multiarea Interconnected Power Systems," *IEEE Access*, vol. 10, pp. 92307-92320, 2022, https://doi.org/10.1109/ACCESS.2022.3201873.

[14] M. Amir and K. Singh, "Chapter 16 - Frequency regulation strategies in renewable energy-dominated power systems: Issues, challenges, innovations, and future trends," *Advanced Frequency Regulation Strategies in Renewable-Dominated Power Systems*, pp. 367-381, 2024, https://doi.org/10.1016/B978-0-323-95054-1.00001-9.

[15] D. Sibtain, T. Rafiq, M. H. Bhatti, S. Shahzad, and H. Kilic, "Frequency stabilization for interconnected renewable based power system using cascaded model predictive controller with fractional order PID controller," *IET Renewable Power Generation*, vol. 17, no. 16, pp. 3836-3855, 2023, https://doi.org/10.1049/rpg2.12885.

[16] V. Kumar and V. Sharma, "Electric vehicle integrated MPC scheme for concurrent control of voltage and frequency in power system network," *Wind Engineering*, vol. 46, no. 2, pp. 529-544, 2022, https://doi.org/10.1177/0309524x211036424.

[17] B. Khokhar and K. P. S. Parmar, "A novel adaptive intelligent MPC scheme for frequency stabilization of a microgrid considering SoC control of EVs," *Applied Energy*, vol. 309, p. 118423, 2022, https://doi.org/10.1016/j.apenergy.2021.118423.

[18] P. Chen, W. Wang, F. Fang, J. Liu, and Z. Chen, "A novel load frequency control strategy for renewable energy power system by coordinating energy storage and thermal power," *Journal of Energy Storage*, vol. 108, p. 115052, 2025, https://doi.org/10.1016/j.est.2024.115052.

[19] M. M. Gulzar, S. T. H. Rizvi, M. Y. Javed, D. Sibtain, and R. S. u. Din, "Mitigating the Load Frequency Fluctuations of Interconnected Power Systems Using Model Predictive Controller," *Electronics*, vol. 8, no. 2, p. 156, 2019, https://doi.org/10.3390/electronics8020156.

[20] M. M. Gulzar, D. Sibtain, M. Al-Dhaifallah, F. Alismail, and M. Khalid, "A new optimal 3° of freedom fractional order proportion integral derivative controller with model predictive controller for frequency regulation in high penetrated renewable based interconnected system," *Computers and Electrical Engineering*, vol. 119, p. 109651, 2024, https://doi.org/10.1016/j.compeleceng.2024.109651.

[21] M. M. Gulzar *et al*., "An Efficient Design of Adaptive Model Predictive Controller for Load Frequency Control in Hybrid Power System," *International Transactions on Electrical Energy Systems*, vol. 2022, no. 1, p. 7894264, 2022, https://doi.org/10.1155/2022/7894264.

[22] D. Sibtain *et al*., "Variable structure model predictive controller based gain scheduling for frequency regulation in renewable based power system," *International Journal of Numerical Modelling: Electronic Networks, Devices and Fields*, vol. 35, no. 4, p. e2989, 2022, https://doi.org/10.1002/jnm.2989.

[23] M. M. Gulzar, D. Sibtain, and M. Khalid, "Cascaded Fractional Model Predictive Controller for Load Frequency Control in Multiarea Hybrid Renewable Energy System with Uncertainties," *International Journal of Energy* Research, vol. 2023, no. 1, p. 5999997, 2023, https://doi.org/10.1155/2023/5999997.

[24] G. Magdy, A. Bakeer, and M. Alhasheem, "Robust decentralized model predictive load-frequency control design for time-delay renewable power systems," *Journal of Emerging Electric Power Systems*, vol. 22, no. 5, pp. 617-628, 2021, https://doi.org/10.1515/ijeeps-2021-0109.

[25] M. A. El-Hameed, M. Saeed, A. Kabbani, and E. Abd El-Hay, "Efficient load frequency controller for a power system comprising renewable resources based on deep reinforcement learning," *Scientific Reports*, vol. 15, no. 1, p. 18379, 2025, https://doi.org/10.1038/s41598-025-03310-2.

[26] M. Ramesh, A. K. Yadav, and P. K. Pathak, "An extensive review on load frequency control of solar-wind based hybrid renewable energy systems," *Energy Sources, Part A: Recovery, Utilization, and Environmental Effects*, vol. 47, no. 1, pp. 8378-8402, 2025, https://doi.org/10.1080/15567036.2021.1931564.

[27] V. V. Yadav and B. Saravanan, "Multimachine stability improvement with hybrid renewable energy systems using a superconducting magnetic energy storage in power systems," *Journal of Energy Storage*, vol. 57, p. 106255, 2023, https://doi.org/10.1016/j.est.2022.106255.

[28] E. A. Rene and W. S. T. Fokui, "A quantum particle swarm optimization-based optimal LQR-PID controller for load frequency control of an isolated power system," *Journal of Engineering and Applied Science*, vol. 70, no. 1, p. 97, 2023, https://10.1186/s44147-023-00271-z.

[29] E. A. Mohamed, M. Aly, A. Elmelegi, E. M. Ahmed, M. Watanabe and S. M. Said, "Enhancement the Frequency Stability and Protection of Interconnected Microgrid Systems Using Advanced Hybrid Fractional Order Controller," *IEEE Access*, vol. 10, pp. 111936-111961, 2022, https://doi.org/10.1109/ACCESS.2022.3216212.

[30] B. Dhanasekaran, J. Kaliannan, A. Baskaran, N. Dey, and J. M. R. S. Tavares, "Load Frequency Control Assessment of a PSO-PID Controller for a Standalone Multi-Source Power System," *Technologies*, vol. 11, no. 1, p. 22, 2023, https://doi:10.3390/technologies11010022.

[31] S. K. Bhatta, S. Mohapatra, P. C. Sahu, S. C. Swain, and S. Panda, "Load frequency control of a diverse energy source integrated hybrid power system with a novel hybridized harmony search-random search algorithm designed Fuzzy-3D controller," *Energy Sources, Part A: Recovery, Utilization, and Environmental Effects*, vol. 47, no. 1, pp. 10839-10862, 2025, https://doi.org/10.1080/15567036.2021.1970860.

[32] D. Yousri, T. S. Babu, and A. Fathy, "Recent methodology based Harris Hawks optimizer for designing load frequency control incorporated in multi-interconnected renewable energy plants," *Sustainable Energy, Grids and Networks*, vol. 22, p. 100352, 2020, https://doi.org/10.1016/j.segan.2020.100352.

[33] Q. Liu and Q. Liu, "Research on Automatic Generation Control System of Photovoltaic Power Station Based on Adaptive PID Control Algorithm," *2020 IEEE 3rd International Conference on Information Systems and Computer Aided Education (ICISCAE)*, pp. 231-236, 2020, https://doi.org/10.1109/ICISCAE51034.2020.9236877.

[34] B. -M. Zamfir, P. -C. Răzuși, S. -C. Olteanu and C. -G. Lupu, "A method for tuning the parameters of a PI controller from an Area Generation Control system," *2025 29th International Conference on System Theory, Control and Computing (ICSTCC)*, pp. 714-718, 2025, https://doi.org/10.1109/ICSTCC66753.2025.11240434.

[35] S. Mishra, U. C. Prusty, R. C. Prusty, and S. Panda, "Novel load frequency control scheme for hybrid power systems employing interline power flow controller and redox flow battery," *Energy Sources, Part A: Recovery, Utilization, and Environmental Effects*, vol. 47, no. 1, pp. 11787-11805, 2025, https://doi.org/10.1080/15567036.2021.1986174.

[36] D. H. Tuan, V. Nguyen Ngoc Thanh, D. Nguyen Chi, and V. H. Pham, "Improving Frequency Control of Multi-Area Interconnected Hydro-Thermal Power System Using PSO Algorithm," *Applied Sciences*, vol. 15, no. 6, p. 2898, 2025, https://doi.org/10.3390/app15062898.

[37] S. K. Ojha and C. O. Maddela, "Load frequency control of a two-area power system with renewable energy sources using brown bear optimization technique," *Electrical Engineering*, vol. 106, no. 3, pp. 3589-3613, 2024, https://10.1007/s00202-023-02143-4.

[38] A. H. Yakout, H. Kotb, H. M. Hasanien and K. M. Aboras, "Optimal Fuzzy PIDF Load Frequency Controller for Hybrid Microgrid System Using Marine Predator Algorithm," *IEEE Access*, vol. 9, pp. 54220-54232, 2021, https://doi.org/10.1109/ACCESS.2021.3070076.

[39] R. Alayi, F. Zishan, S. R. Seyednouri, R. Kumar, M. H. Ahmadi, and M. Sharifpur, "Optimal Load Frequency Control of Island Microgrids via a PID Controller in the Presence of Wind Turbine and PV," *Sustainability*, vol. 13, no. 19, p. 10728, 2021, https://doi.org/10.3390/su131910728.

[40] A. K. Mishra, P. Sharma, H. Siguerdidjane, P. Mishra, and H. D. Mathur, "Maiden Application of Integral-Tilt Integral Derivative with Filter (I-TDN) Control Structure for Load Frequency Control," *IFAC-PapersOnLine*, vol. 55, no. 34, pp. 72-77, 2022, https://doi.org/10.1016/j.ifacol.2022.11.310.

[41] M. M. Gulzar, M. Iqbal, S. Shahzad, H. A. Muqeet, M. Shahzad, and M. M. Hussain, "Load Frequency Control (LFC) Strategies in Renewable Energy-Based Hybrid Power Systems: A Review," *Energies*, vol. 15, no. 10, p. 3488, 2022, https://doi:10.3390/en15103488.

[42] J. Zhou, Y. Jia, P. Yong, Z. Liu, and C. Sun, "Robust deep Koopman model predictive load frequency control of interconnected power systems," *Electric Power Systems Research*, vol. 226, p. 109948, 2024, https://doi.org/10.1016/j.epsr.2023.109948.

[43] J. Zhang, P. Wei and B. Qin, "Automatic Generation Control Design of Doubly-Fed Induction Generator Integrated Power System Based on Distributed Model Predictive Control," *2023 5th International Conference on Power and Energy Technology (ICPET)*, pp. 736-741, 2023, https://doi.org/10.1109/ICPET59380.2023.10367507.

[44] P. Wang, J. Guo, F. Cheng, Y. Gu, F. Yuan, and F. Zhang, "A MPC-based load frequency control considering wind power intelligent forecasting," *Renewable Energy*, vol. 244, p. 122636, 2025, https://doi.org/10.1016/j.renene.2025.122636.

[45] Z. Hu, K. Zhang, R. Su and R. Wang, "Robust Cooperative Load Frequency Control for Enhancing Wind Energy Integration in Multi-Area Power Systems," *IEEE Transactions on Automation Science and Engineering*, vol. 22, pp. 1508-1518, 2025, https://doi.org/10.1109/TASE.2024.3367030.

[46] A. M. Taher *et al*., "Optimal model predictive control of energy storage devices for frequency stability of modern power systems," *Journal of Energy Storage*, vol. 57, p. 106310, 2023, https://doi.org/10.1016/j.est.2022.106310.

[47] Z. Wang, Y. Liu, Z. Yang, and W. Yang, "Load Frequency Control of Multi-Region Interconnected Power Systems with Wind Power and Electric Vehicles Based on Sliding Mode Control," *Energies*, vol. 14, no. 8, p. 2288, 2021, https://doi:10.3390/en14082288.

[48] Z. Deng, C. Xu, Z. Huo, X. Han, and F. Xue, "Sliding Mode Based Load Frequency Control and Power Smoothing of Power Systems with Wind and BESS Penetration," *Machines*, vol. 10, no. 12, p. 1225, 2022, https://doi:10.3390/machines10121225.

[49] A. Kumar, M. N. Anwar, and S. Kumar, "Sliding mode controller design for frequency regulation in an interconnected power system," *Protection and Control of Modern Power Systems*, vol. 6, no. 1, pp. 1-12, 2021, https://10.1186/s41601-021-00183-1.

[50] A.-T. Tran, V. V. Huynh, and T. L.-T. Tran, "Load Frequency Control Design for Complex Power Systems Implementing Integral Single-Phase Sliding Mode Control," *Engineering, Technology & Applied Science Research*, vol. 15, no. 1, pp. 19802-19808, 2025, https://doi.org/10.48084/etasr.9323.

[51] H. H. Alhelou, N. Nagpal, N. Kassarwani and P. Siano, "Decentralized Optimized Integral Sliding Mode-Based Load Frequency Control for Interconnected Multi-Area Power Systems," *IEEE Access*, vol. 11, pp. 32296-32307, 2023, https://doi.org/10.1109/ACCESS.2023.3262790.

[52] Z. Wang and Y. Liu, "Adaptive Terminal Sliding Mode Based Load Frequency Control for Multi-Area Interconnected Power Systems With PV and Energy Storage," *IEEE Access*, vol. 9, pp. 120185-120192, 2021, https://doi.org/10.1109/ACCESS.2021.3109141.

[53] D. H. Tuan, J. Pidanic, V. v. Huynh, V. H. Duy and N. H. K. Nhan, "Sliding Mode Without Reaching Phase Design for Automatic Load Frequency Control of Multi-Time Delays Power System," *IEEE Access*, vol. 12, pp. 110052-110063, 2024, https://doi.org/10.1109/ACCESS.2024.3441092.

[54] G. Mustafa, H. Wang, and M. D. Masum, "A New Model-Free Adaptive Integral Sliding Mode Control for Interconnected Power Systems Load Frequency Control," *International Journal of Robust and Nonlinear Control*, vol. 35, no. 5, pp. 1792-1808, 2025, https://doi.org/10.1002/rnc.7756.

[55] A. Dev *et al*., "Enhancing load frequency control and automatic voltage regulation in Interconnected power systems using the Walrus optimization algorithm," *Scientific Reports*, vol. 14, no. 1, p. 27839, 2024, https://10.1038/s41598-024-77113-2.

[56] Y. O. M. Sekyere, F. B. Effah, and P. Y. Okyere, "Optimally tuned cascaded FOPI-FOPIDN with improved PSO for load frequency control in interconnected power systems with RES," *Journal of Electrical Systems and Information Technology*, vol. 11, no. 1, p. 25, 2024, https://10.1186/s43067-024-00149-x.

[57] V. Patel, D. Guha, and S. Purwar, "Neural network aided fractional-order sliding mode controller for frequency regulation of nonlinear power systems," *Computers & Electrical Engineering*, vol. 96, p. 107534, 2021, https://doi.org/10.1016/j.compeleceng.2021.107534.

[58] A. Otsuka, "Regional data on electricity consumption and electricity prices in Japan," *Data in Brief*, vol. 50, p. 109467, 2023, https://doi.org/10.1016/j.dib.2023.109467.

[59] A. F. Ghaliba and A. A. Oglah, "Design and Implementation of a Fuzzy Logic Controller for Inverted Pendulum System Based on Evolutionary Optimization Algorithms," *Engineering and Technology Journal*, vol. 38, no. 3, pp. 361-374, 2020, https://scispace.com/pdf/design-and-implementation-of-a-fuzzy-logic-controller-for-1iyhhgjpbn.pdf.

[60] M. T. Muhssin, M. N. Ajaweed, and S. K. Khalaf, "Optimal control of underwater vehicle using LQR controller driven by new matrix decision control algorithm," *International Journal of Dynamics and Control*, vol. 11, no. 6, pp. 2911-2923, 2023, https://10.1007/s40435-023-01186-6.